Optimization of the conversion efficiency and evaluation of the noise figure of an optical frequency converter based on a dual-pump fiber phase sensitive amplifier

Debanuj Chatterjee, Yousra Bouasria, Fabienne Goldfarb, Yassine Hassouni, Fabien Bretenaker

Research Article | Vol. 30, No. 25 / 5 Dec 2022 / Optics Express 45676
Optics EXPRESS

Optimization of the conversion efficiency and evaluation of the noise figure of an optical frequency converter based on a dual-pump fiber phase sensitive amplifier

DEBANUJ CHATTERJEE,[1,2] YOUSRA BOUASRIA,[3,4] FABIENNE GOLDFARB,[1] YASSINE HASSOUNI,[3] AND FABIEN BRETENAKER[1,*]

[1] Université Paris-Saclay, CNRS, ENS Paris-Saclay, CentraleSupélec, LuMIn, Gif-sur-Yvette, France
[2] Indian Institute of Technology Madras, Chennai 600036, India
[3] Equipe Sciences de la Matière et du Rayonnement (ESMaR), Faculté des Sciences, Université Mohammed V, Rabat, Morocco
[4] QUANTIC team, INRIA de Paris, 2 Rue Simone Iff, 75012 Paris, France
[*] Fabien.bretenaker@universite-paris-saclay.fr

Abstract: We propose a new architecture of phase sensitive optical frequency converter based on dual-pump phase sensitive amplification in a highly nonlinear fiber. This frequency converter allows generation of extra tones through nonlinear four-wave mixing between two strong pumps and an input tone. The frequency channel to which the input tone is converted can be chosen by adjusting the phase of the input signal. The conversion efficiency and extinction ratio of this frequency converter are predicted and optimized and its noise figure is calculated using a numerical approach based on the nonlinear Schrödinger equation. A semi-classical noise figure calculation for this approach was used and validated using an analytical fully quantum calculation based on the multi-wave model.

1. Introduction

The ever increasing growth of demand for higher network capacity and better performance of communication systems is posing critical challenges for optical communication systems. In recent years, all-optical signal processing (AOSP) has shown remarkable potential for improving optical networks by realizing various signal processing functionalities and providing processing speeds beyond the limits of its electronic counterparts. In this respect, the recent developments in the study of fiber-optic phase sensitive amplifiers (PSA) has opened up new avenues in the development of future fiber-optic AOSP modalities [1–4]. Thanks to its unique phase sensitive property, several breakthroughs have been reported including signal regeneration [5], low-noise amplification [6], etc., to name only a few.

Recently, applications of PSA towards AOSP with respect to frequency and modulation format conversion of data carrying optical signals have been reported. The key idea behind this was to use phase-sensitive four-wave mixing (FWM) interactions between a signal and multiple pumps to simultaneously separate the two complex quadratures of the signal by converting them to different frequencies. Such a scheme was experimentally implemented by Webb *et al.* using a semiconductor optical amplifier (SOA) as the nonlinear medium [7,8]. However, AOSP based on SOAs are much slower compared to FWM in fibers since SOAs are limited by the response time of the carriers in the SOA [9,10]. It has been shown experimentally by Da Ros *et al*, that the use of highly nonlinear fibers (HNLF) can be more efficient for ultrafast quadrature-dependent frequency conversion of data modulated signals. In their study, they demonstrated the conversion of the two complex quadratures of a quadrature phase-shift keying (QPSK) signal to two binary

#471087 https://doi.org/10.1364/OE.471087
Journal © 2022 Received 20 Jul 2022; revised 13 Sep 2022; accepted 3 Oct 2022; published 1 Dec 2022

Optics EXPRESS

phase-shift keying (BPSK) signals utilizing FWM among four CW pumps and a signal [2]. As a follow up of this work, Baillot *et al.* have shown theoretically and experimentally that it is in fact possible to achieve a phase sensitive frequency conversion (PSFC) in a HNLF using only three pump waves [3]. In all these previous demonstrations, the implementation of the PSFC required careful adjustment of many parameters of the system, including power levels and phases of the three or four pump waves, thus adding some complexity to the system. Therefore, in the present article, we investigate a simpler PSFC configuration involving only two pump waves and the frequency channel to be converted. This scheme is based on a multi-wave PSA model and is thus expected to reduce the system complexity to a large extent. We thus numerically investigate the conversion efficiency and noise figure (NF) of such a scheme and determine the system dependence on relevant parameters.

Since the PSFC architecture proposed here relies on nonlinear interaction between several waves, the present work is strongly linked to studies of multi-wave models in PSAs. Indeed, different types of multi-wave models in general have been extensively studied in order to predict and understand the gain and noise performances of multi-wave PSAs [11–17]. The seven-wave model in particular was comprehensively investigated numerically by Xie *et al.* who predicted the possibility of signal gain enhancements [18] and applications to signal regeneration [19]. Also, in a previous work, we proposed an accurate analytical description of the dynamics of such a seven-wave PSA under the strong pump approximation [4]. Furthermore, in order to answer the question whether gain enhancements in a seven-wave PSA are accompanied with degradation of the PSA noise figure or not, both quantum [16,17] and semi-classical [20,21] approaches were developed based on the multi-wave model. Although these various approaches were used for the investigation of noise properties of a PSA using the multi-wave model, a comprehensive comparison between the semi-classical and quantum approaches is absent from the literature to the best of our knowledge, thus constituting a second motivation for the present work.

Consequently, the first goal of this paper is to establish both quantum and semi-classical approaches for NF calculations in a dual-pump PSA configuration. For the quantum approach, we perform the NF calculations by quantizing the classical analytical solutions derived in Ref. [4]. We note here that under the strong pump approximation, the analytical solutions of the seven-wave PSA effectively reduce to a five-wave system as shown in Ref. [4]. In the semi-classical approach, we solve the propagation of the waves numerically by solving the nonlinear Schrödinger equation (NLSE), and evaluate the NF adapting an approach akin to Ref. [21]. Henceforth we utilize these two methods for NF calculation of a dual-pump PSA in the case of a short fiber, implying a weak nonlinearity, where both the quantum and semi-classical approaches are valid. After a validation with the fully quantum approach in this latter case, the semi-classical NF calculation method is then extended to the case of a longer fiber, with a stronger nonlinearity, where a fully quantum approach is absent.

The second goal of this paper is to propose a novel dual-pump PSFC scheme in the framework of the five-wave model [22]. In fact we also investigate the dependence of the conversion efficiency of the PSFC on the pump-pump wavelength separation, fiber length and the signal wavelength detuning from the fiber zero-dispersion wavelength, for an optimized performance. Furthermore, for the PSFC, we repeat the NF evaluation routine using the semi-classical approach, and investigate the noise transferred from the input signal to the frequency converted waves.

This article is organized as follows. In Section 2 we introduce the theoretical framework of the analytical five-wave PSA, and discuss the possibility to exploit this five-wave scheme as a dual-pump PSFC. In Section 3, we first elucidate the quantum and semi-classical NF calculation methods, then we compare the gain and NF of a dual-pump PSA based on these methods. Thereafter in Section 4 we investigate the conversion efficiency and NF of the dual-pump PSFC scheme with respect to some relevant system parameters. Finally in Section 5 we draw the conclusion and project some future perspectives.

Optics EXPRESS

2. Five-wave model for phase sensitive frequency conversion

This section presents the five-wave model that is used to describe the operation of the phase sensitive frequency converter. To be valid, this model requires that the system nonlinearity is weak enough for extra waves beyond these five waves to be negligible. Extension to the case of stronger nonlinearities will be performed in Section 3.2 using the NLSE. The present section in particular discusses which approximations are necessary to obtain analytical expressions for the input-output relations for the amplitudes of the different waves. Based on this, we then show how this dual-pump system can, beyond its phase sensitive amplification property, be used also as a phase sensitive frequency converter.

2.1. Five-wave model for the phase sensitive amplifier (PSA)

Launching two strong pump waves with a signal wave inside a nonlinear fiber leads to the creation of extra waves by cascaded FWM interaction. To accurately consider the coupled dynamics of all these waves, ideally one should study the evolution of the whole frequency spectrum through the fiber. However, to simplify the situation, a reasonable approximation can be made by truncating the system to only a few discrete waves. The slowly varying complex amplitude A_j of the jth wave can be simplified into an ordinary differential equation [23]:

$$\frac{dA_j}{dz} = i\gamma\left[|A_j|^2 A_j + 2\sum_{l\neq j=-k}^{k}|A_l|^2 A_j + \sum_{\substack{m,n,p=-k,\\ \omega_m+\omega_n-\omega_p=\omega_j}}^{k} A_m A_n A_p^* e^{i\Delta\beta_{mnpj}z}\right], \tag{1}$$

where we consider evolution of $2k+1$ waves with the index j running from $-k$ to k. $\Delta\beta_{mnpj} = \beta(\omega_m) + \beta(\omega_n) - \beta(\omega_p) - \beta(\omega_j)$ is the linear phase mismatch coefficient where $\beta(\omega_j)$ is the propagation constant at an angular frequency ω_j, γ is the nonlinear coefficient of the fiber, z is the propagation distance. In the particular case of $k = 3$, we obtain the so-called seven-wave model schematized in Fig. 1. This model involves seven waves, which are equally spaced in frequency: the two pumps, a degenerate signal and idler, two so-called high-order idlers (HOIs), and two so-called high-order pumps (HOPs). Of course, the validity of this model is limited to the cases where the nonlinearity is not too strong, allowing one to neglect higher order waves. The key assumptions of our analytical model are reiterated below :

(1) Dispersion is considered up to second order in the Taylor series expansion of $\beta(\omega)$.

(2) The input phases of the pumps are 0 rads.

(3) The pumps are considered undepleted along the fiber length and are much stronger in power compared to the other waves.

(4) The undepleted strong pump approximation also lead to decoupling of the HOPs from the signal and HOIs [4]. Thus effectively we are left with only five waves ($k = 2$ in Eq. (1); two pumps, signal and two HOIs) to predict the evolution of the signal along the fiber.

In the existing literature, numerical methods are usually used to solve Eq. (1) and analyze, for example, the signal gain spectrum [18]. Obtaining analytical solutions is complex and still an unsolved problem in general, especially when the fiber dispersion and pump depletion are considered. In fact inclusion of pump depletion in the model leads to solutions in terms of Jacobian elliptic functions, that are practically intractable due to a lack of closed form expressions [24]. However, in the regime where pump depletion can be neglected, an attempt has been made to arrive at a solution in [4], and input-output relations between the interacting waves have been derived to describe the operation of this device as a PSA. This derivation uses the no pump depletion approximation to break down the seven-wave system into three subsystems. This leads

Optics EXPRESS

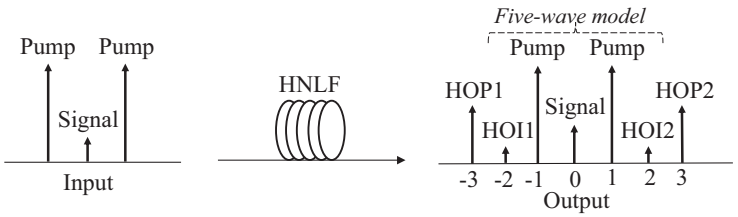

Fig. 1. Schematic representation of the seven-wave model. The index j of the different waves are shown in the output spectrum below the corresponding waves. HNLF : highly nonlinear fiber, HOI : high-order idler, HOP : high-order pump.

in particular to a decoupling of the HOPs from the signal and HOIs. The system thus effectively involves only five waves. The resulting five-wave model thus considers only the coupling between the pumps, signal, and HOIs, and possesses analytical solutions [4]. These solutions are found to agree satisfactorily with more general numerical simulations when the nonlinear phase shift γPL, where γ is the fiber nonlinear coefficient, L the fiber length, and P the power of the pumps, remains significantly smaller than 1 rad. In this parameter range, the influence of the HOPs on the signal can be neglected as their evolution is independent from the signal and the HOIs.

According to [4], the solution of this five-wave model relating the output amplitudes of the modes to the inputs is then given by:

$$\begin{pmatrix} B_0 \\ B_0^* \\ B_{-2} \\ B_{-2}^* \\ B_2 \\ B_2^* \end{pmatrix} = \begin{pmatrix} \mu_{11} & \mu_{12} & \mu_{13} & \dots & \dots & \mu_{16} \\ \mu_{21} & \mu_{22} & \dots & \dots & \dots & \mu_{26} \\ \mu_{31} & \vdots & \ddots & \ddots & \ddots & \vdots \\ \mu_{41} & \vdots & \ddots & \ddots & \ddots & \vdots \\ \mu_{51} & \vdots & \ddots & \ddots & \ddots & \vdots \\ \mu_{61} & \dots & \dots & \dots & \dots & \mu_{66} \end{pmatrix} \begin{pmatrix} A_0 \\ A_0^* \\ A_{-2} \\ A_{-2}^* \\ A_2 \\ A_2^* \end{pmatrix}, \tag{2}$$

where A_j and B_j are the amplitudes of wave j at the input and output of the fiber, respectively. Index 0 denotes the signal and indices -2 and 2 refer to the HOI1 and HOI2, respectively (see Fig. 1). The coefficients μ_{kl} of the transfer matrix $M = [\mu_{kl}]$, with $k, l = 1, ..6$, are in general complex. Their explicit expressions are given in the Supplemental document.

From Eq. (2), the signal gain for this PSA is expressed as:

$$G_{0,\mathrm{PSA}} = \frac{|B_0|^2}{|A_0|^2} = |\mu_{11}|^2 + |\mu_{12}|^2 + 2|\mu_{11}||\mu_{12}| \cos\Theta\,, \tag{3}$$

where $\Theta = 2\theta_0 + \theta_{11} - \theta_{12}$ is the relative phase between the signal and the two pumps at the fiber input. Here, θ_{11} and θ_{12} are the arguments of the complex coefficients μ_{11} and μ_{12}, respectively, and θ_0 is the phase of the signal at the input.

2.2. Application to the phase sensitive frequency converter (PSFC)

As stated in the introduction, the presence of several waves at the output of the PSA opens interesting perspectives in terms of frequency conversion. The five-wave scheme can be transformed into a frequency converter following two different strategies. Indeed, along with the two pumps labeled -1 and 1, the frequency to be converted can be launched either as the signal

Optics EXPRESS

(see Fig. 1) or as the high-order idler HOI1 (see Fig. 2). In both cases, the conversion efficiency from input channel i to output channel j is defined as:

$$\mathrm{CE}_j = \frac{|B_j|^2}{|A_i|^2}\,. \tag{4}$$

When we consider conversion from the signal frequency to the HOIs (see Fig. 1), the symmetrical allocation of the waves leads to generation of HOI1 and HOI2 with equal powers. The efficiency of this conversion is phase sensitive, but, when dispersion is neglected, there is no way to favor one of the HOIs with respect to the other. Consequently, the symmetric scheme of Fig. 1 is better suited for phase sensitive parametric amplification of the signal than to frequency conversion towards a single channel.

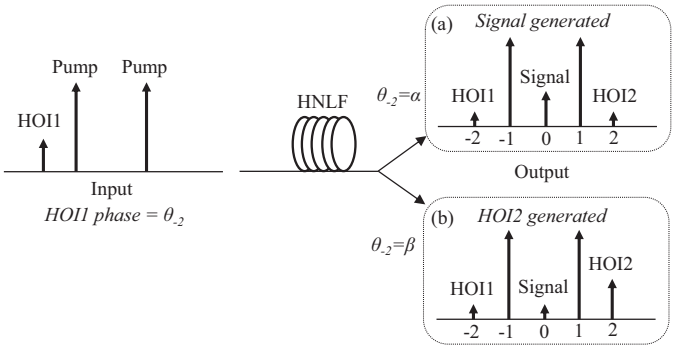

Fig. 2. Phase sensitive frequency conversion (PSFC) scheme where the HOI1 is launched together with the two pumps at the input of the fiber. At HNLF output, signal is generated when $\theta_{-2} = \alpha$ (a), idler is generated when $\theta_{-2} = \beta$ (b), where θ_{-2} is input HOI1 phase. $\alpha \neq \beta$.

On the contrary, when we consider the asymmetric scheme of Fig. 2, in which the input wave is launched in HOI1 along with the two pumps, we can expect the five-wave scheme to be capable of operating as a frequency converter in which the privileged output frequency, either the signal (Fig. 2(a)) or HOI2 (Fig. 2(b)), can be chosen by tuning the input phase difference between the waves. This would constitute a very interesting scheme for applications, in which only two pumps are necessary to obtain a frequency tunable frequency converter.

The conversion efficiencies from HOI1 to the signal or to HOI2 are then given from Eqs. (2, 4) by:

$$\mathrm{CE}_j = \frac{|B_j|^2}{|A_{-2}|^2} = |\mu_{k3}|^2 + |\mu_{k4}|^2 + 2|\mu_{k3}||\mu_{k4}|\cos\Theta\,, \tag{5}$$

where $k = 1$ or 5 and $j = 0$ or 2, respectively. Here, the relative phase is defined as $\Theta = 2\theta_{-2} + \theta_{k3} - \theta_{k4}$. With $k = 3$ and $j = -2$, this expression provides the gain experienced by HOI1.

3. Fully quantum and semi-classical approaches to the noise figure

The preceding section has detailed how we calculate the conversion efficiency based on a classical description of the fields. Another important parameter is the excess noise added to the converted field. In principle, this extra noise must be calculated using a quantum description of the fields. However, this approach is very cumbersome, and we thus search whether a much simpler semi-classical approach could be used or not. Thus, in order to assess the domain of validity of such a semi-classical approach, we first perform in the present section a comparison between

Optics EXPRESS

the different approaches in the well known case of a PSA. Once validated, the semi-classical approach will be applied to the PSFC in Section 4.

Consequently, the present section details the quantum and semi-classical approaches that are used to calculate the noise properties of the optical amplifier. The quantum approach is then applied to the five-wave model described in the preceding section, and compared with the semi-classical approach applied to the NLSE.

3.1. Quantum-mechanical approach based on the five-wave model

In the quantum derivation of the amplifier NF [25–29], the light electric field is represented by an operator. The fact that the quadratures of this field do not commute leads to an intrinsic quantum noise, which is inevitable in order to respect Heisenberg inequalities. In our case, the quantum noise added to the signal by the amplifier can be quantified using the NF defined as the ratio between the signal-to-noise ratios (SNRs) at the input and output of the amplifier:

$$\mathrm{NF} = \frac{\mathrm{SNR}_{\mathrm{in}}}{\mathrm{SNR}_{\mathrm{out}}} = \frac{\langle N\rangle_{\mathrm{in}}^2}{\langle \Delta N^2\rangle_{\mathrm{in}}} \cdot \frac{\langle \Delta N^2\rangle_{\mathrm{out}}}{\langle N\rangle_{\mathrm{out}}^2}\,. \tag{6}$$

where the SNR, chosen here in terms of photon number, is defined as the square of the mean photon number $\langle N\rangle^2$ divided by the photon number variance $\langle \Delta N^2\rangle$.

Equation (6) can be applied to calculate the NF in combination with the classical input-output relations given by Eq. (2). To apply these relations to the quantum fields, the classical amplitudes A_j (and B_j) of mode j, and their complex conjugates A_j^* (and B_j^*) have to be replaced by the annihilation and creation operators $\hat{a}_j$ and $\hat{a}_j^\dagger$ ($\hat{b}_j$ and $\hat{b}_j^\dagger$), respectively.

By using the Mathematica code given in Ref. [16], the NF for the signal ($j = 0$) is found to be, under the large-photon number approximation (see the supplementary document for more details):

$$\begin{aligned}
\mathrm{NF}_0 = {} & \frac{1}{\left(|\mu_{11}|^2 + |\mu_{12}|^2 + 2\,|\mu_{12}|\,|\mu_{11}|\cos\left(2\theta_0 + \theta_{11} - \theta_{12}\right)\right)^2} \times \Big\{ |\mu_{11}|^4 + |\mu_{12}|^4 + 6\,|\mu_{12}|^2\,|\mu_{11}|^2 \\
& + |\mu_{13}|^2\,|\mu_{11}|^2 + |\mu_{14}|^2\,|\mu_{11}|^2 + |\mu_{15}|^2\,|\mu_{11}|^2 + |\mu_{16}|^2\,|\mu_{11}|^2 + |\mu_{12}|^2\,|\mu_{13}|^2 + |\mu_{12}|^2\,|\mu_{14}|^2 \\
& + |\mu_{12}|^2\,|\mu_{15}|^2 + |\mu_{12}|^2\,|\mu_{16}|^2 + 4\,|\mu_{12}|\,|\mu_{11}|^3\cos\left(\theta_{11} - \theta_{12} + 2\theta_0\right) \\
& + 2\,|\mu_{13}|\,|\mu_{14}|\,|\mu_{11}|^2\cos\left(2\theta_{11} - \theta_{13} - \theta_{14} + 2\theta_0\right) + 2\,|\mu_{15}|\,|\mu_{16}|\,|\mu_{11}|^2\cos\left(2\theta_{11} - \theta_{15} - \theta_{16} + 2\theta_0\right) \\
& + 4\,|\mu_{12}|^3\,|\mu_{11}|\cos\left(\theta_{11} - \theta_{12} + 2\theta_0\right) + 2\,|\mu_{12}|\,|\mu_{13}|^2\,|\mu_{11}|\cos\left(\theta_{11} - \theta_{12} + 2\theta_0\right) \\
& + 2\,|\mu_{12}|\,|\mu_{14}|^2\,|\mu_{11}|\cos\left(\theta_{11} - \theta_{12} + 2\theta_0\right) + 2\,|\mu_{12}|\,|\mu_{15}|^2\,|\mu_{11}|\cos\left(\theta_{11} - \theta_{12} + 2\theta_0\right) \\
& + 2\,|\mu_{12}|\,|\mu_{16}|^2\,|\mu_{11}|\cos\left(\theta_{11} - \theta_{12} + 2\theta_0\right) + 2\,|\mu_{12}|^2\,|\mu_{13}|\,|\mu_{14}|\cos\left(-2\theta_{12} + \theta_{13} + \theta_{14} + 2\theta_0\right) \\
& + 2\,|\mu_{12}|^2\,|\mu_{15}|\,|\mu_{16}|\cos\left(-2\theta_{12} + \theta_{15} + \theta_{16} + 2\theta_0\right) + 4\,|\mu_{12}|\,|\mu_{13}|\,|\mu_{14}|\,|\mu_{11}|\cos\left(\theta_{11} + \theta_{12} - \theta_{13} - \theta_{14}\right) \\
& + 4\,|\mu_{12}|\,|\mu_{15}|\,|\mu_{16}|\,|\mu_{11}|\cos\left(\theta_{11} + \theta_{12} - \theta_{15} - \theta_{16}\right) \Big\},
\end{aligned} \tag{7}$$

where $\mu_{kl} = |\mu_{kl}|e^{i\theta_{kl}}$.

Equation (7) for the signal NF is calculated using the first row of the transfer matrix (Eq. (2)) relating the output signal mode to the input signal ($k = 1, 2$) and high-order idler modes ($l = 3, 4, 5, 6$). The dependence on the pump powers is implicitly introduced in the coefficients μ_{kl} (see the expressions of these coefficients in the supplemental document), because the pump waves are not counted as quantum modes. Indeed, the pumps are treated as classical fields due to the pump non-depletion assumption considered in the analytical solution of the 5-wave model.

The different terms involved in Eq. (7) come from the nonlinear interactions between the signal mode, high-order idler modes and their complex conjugates. These interactions are responsible

Optics EXPRESS

for energy and noise transfer among the different modes. For example, the terms containing only $|\mu_{11}|$ and/or $|\mu_{12}|$ corresponds to the nonlinear coupling between the signal and itself or between the signal and its complex conjugate. The terms of the form $|\mu_{11}\mu_{1l}|$ and $|\mu_{12}\mu_{1l}|$, with $l = 3, 4, 5, 6$ corresponds to the nonlinear coupling among the signal and high-order idlers.

The remaining terms of the equation that contain the cosine function and depend on the input signal phase θ_0 confirm the phase sensitivity of our five wave PSA. This sensitivity implies that with appropriate choices of θ_0, the vacuum noises can be transferred from the high-order idler modes to the signal mode or flowed back from the signal to the HOIs through multiple FWM interactions.

Some examples of NF calculations using this quantum-mechanical derivation will be given in Section 3.3. But before this we describe in the following subsection the semi-classical description to which these results will be compared.

3.2. Semi-classical approach based on the nonlinear Schrödinger equation (NLSE)

Although the noise of an optical amplifier can only be fully understood by adopting a quantum-mechanical treatment, it is possible to deal with the noise properties within the framework of the semi-classical approach. Along this approach, the quantum noise is mimicked by a Gaussian noise added to the classical complex field amplitude. This additive noise has a zero mean and a variance corresponding to one half of the energy of a photon.

In the literature, this semi-classical approach has been broadly used for calculating the signal NF in the case of the fundamental three-wave model [30–32]. Recently, it has been used as well for calculating the signal noise in the framework of the seven-wave model of Fig. 1 [21], evidencing the impact of the HOIs on the signal noise figure. The vacuum noise entering the HOPs was found to have a negligible influence compared to the one entering the HOIs. The extra noise falling into the signal due to its interaction with the HOIs was modeled semi-classically by adding a small amount of power, mimicking vacuum fluctuations, at the input of the HOIs. The interaction between the incident "vacuum fluctuations" injected in the HOIs and the pumps and signal along the fiber was evaluated by carrying out numerical simulations of the seven-wave coupled equations. By solving the whole set of equations, and by calculating semi-classically the intensity noise of the signal, a NF expression of the signal was obtained [21].

Here, we follow a similar numerical approach as in Ref. [21], however instead of solving the coupled seven-wave equation, we solve the corresponding NLSE numerically. The reason behind this choice is that the NLSE is applicable to situations where the nonlinearity is strong, in which coupled wave models fail. We model the signal amplitude at the output of the PSA of gain G_0 as:

$$A_{0,\text{out}} = \sqrt{G_0}A_{0,in} + \xi_0\delta A_{0,in} + \xi_{-2}\delta A_{-2,in} + \xi_2\delta A_{2,in} \tag{8}$$

where $A_{0,in}$ is the input signal amplitude and $\delta A_{0,in}$ is the input vacuum fluctuations of the signal. The coefficients ξ_{-2} and ξ_2 represent the strength of transfer of input vacuum fluctuations $\delta A_{-2,in}$ and $\delta A_{2,in}$ injected into the high-order idlers to the signal. For standard input vacuum fluctuations, we have $\langle \delta A_{j,in} \rangle = 0$, $\langle \delta A_{j,in}^2 \rangle = 0$ and $\langle |\delta A_{j,in}|^2 \rangle = h\nu_j/2$, where h is Planck's constant and ν_j is the optical frequency of wave j.

By using Eq. (8), we calculate the intensity noise of the signal, and we obtain the following NF expression (see supplemental information for details):

$$\text{NF}_0 = \frac{1}{4{G_0}^2 P_{0,\text{in}}}\left[\left(\frac{\partial P_{0,\text{out}}}{\partial\sqrt{P_{0,\text{in}}}}\right)^2 + \left(\frac{\partial P_{0,\text{out}}}{\partial\sqrt{P_{-2,\text{in}}}}\right)^2 + \left(\frac{\partial P_{0,\text{out}}}{\partial\sqrt{P_{2,\text{in}}}}\right)^2\right], \tag{9}$$

where G_0 is the PSA signal gain, and $P_{0,\text{in}}$ is the input signal power.

The first term in Eq. (9) corresponds to the signal NF when only the fundamental three waves (signal and two pumps) are considered, where the partial derivative $\partial P_{0,\text{out}}/\partial\sqrt{P_{0,\text{in}}}$ holds for

Optics EXPRESS

the power differential in the output signal due to fluctuations in its input. Of course, in the case where the input signal and its fluctuations have the same phase, ξ_0 in Eq. (8) is simply equal to $\sqrt{G_0}$. Then Eq. (9) simplifies to become:

$$\mathrm{NF}_0 = 1 + \frac{1}{4{G_0}^2 P_{0,\mathrm{in}}}\left[\left(\frac{\partial P_{0,\mathrm{out}}}{\partial\sqrt{P_{-2,\mathrm{in}}}}\right)^2 + \left(\frac{\partial P_{0,\mathrm{out}}}{\partial\sqrt{P_{2,\mathrm{in}}}}\right)^2\right]. \tag{10}$$

However, in the following, we keep Eq. (9), which is more general. The second and third terms in Eq. (9) are associated with the high-order idlers. They represent the extra amount of noise added to the signal due to its interaction with the HOIs. In other words, they describe the transfer to the signal of the vacuum fluctuations injected in the HOIs at the fiber input. The efficiency of this transfer is given by the partial derivatives $\partial P_{0,\mathrm{out}}/\partial\sqrt{P_{-2,\mathrm{in}}}$ and $\partial P_{0,\mathrm{out}}/\partial\sqrt{P_{2,\mathrm{in}}}$ in Eq. (9), where $P_{0,\mathrm{out}}$ is the output signal power and $P_{-2,\mathrm{in}}$ and $P_{2,\mathrm{in}}$ are the small input powers mimicking the vacuum fluctuations entering HOI1 and HOI2, respectively, at the fiber input.

The three partial derivatives in Eq. (9) can be calculated numerically by injecting different amounts of vacuum noise powers at the input of the signal, HOI1 and HOI2 waves, and evaluating the extra noise power it adds compared to when no vacuum noise is added at the input of the waves. In Ref. [21], these partial derivative terms were simulated using the coupled-wave equations in order to find out the impact of the input vacuum noise entering each wave on the signal NF. However, when the nonlinearity of the fiber is large, higher-order waves become dominant in the evolution process of the interacting waves; hence, the NLSE is preferred for more accurate results [33]. Let us remind that it is given by:

$$\frac{\partial A}{\partial z} + \frac{i\beta_2}{2}\frac{\partial^2 A}{\partial T^2} - \frac{\beta_3}{6}\frac{\partial^3 A}{\partial T^3} - \frac{i\beta_4}{24}\frac{\partial^4 A}{\partial T^4} - i\gamma|A|^2 A = 0, \tag{11}$$

where $A(z,T)$ is the slowly varying envelope of the time domain complex amplitude of the wave propagating along z, $T = t - \beta_1 z$ is the retarded time, and the β_n's are the successive dispersion terms of order n.

Consequently, in Subsection 3.3, we compare the NF values obtained by means of the NLSE with the fully quantum approach of Subsection 3.1.

3.3. Comparison between the approaches

In this subsection, we compare the values of the noise figure obtained according to the fully quantum approach of Eq. (7) with the semi-classical calculation summarized in the preceding subsection. We consider a standard HNLF with $\gamma = 11.3\,\mathrm{W}^{-1}.\mathrm{km}^{-1}$, a zero-dispersion wavelength $\lambda_{\mathrm{ZDW}} = 1547.5$ nm, and dispersion slope $D^{'} = 0.017\,\mathrm{ps.nm}^{-2}.\mathrm{km}^{-1}$. We choose a pump power P equal to 20 dBm, signal power of −20 dBm and a signal wavelength $\lambda_0 = 1557.5$ nm. The fiber dispersion in the analytical five-wave model is taken into account up to the second-order derivative of $\beta(\omega)$, while it is considered up to the fourth-order derivative of $\beta(\omega)$ in the NLSE. We focus on the anomalous dispersion region because it is the one in which the five-wave model predicts an excess gain with respect to the three-wave model [4], a situation which is particularly attractive for applications. A standard split step Fourier method (SSFM) algorithm was used to solve the NLSE with a step size of 10 m and frequency resolution of 67 MHz.

Figure 3 compares two values of the overall nonlinearity of the system, obtained by changing the value of the fiber length: $L = 100$ m (in Fig. 3(a)) and $L = 720$ m (in Fig. 3(b)). In each case, we plot the evolution of the maximum gain versus pump-pump wavelength separation $\Delta\lambda_{\mathrm{PP}}$. The maximum gain is obtained by scanning the phase of the input signal and keeping the value that maximizes the gain. The wavelength allocation of the different waves is also defined by the wavelength offset of the signal with respect to the zero-dispersion wavelength, which, in the case of Fig. 3, is equal to $\delta\lambda_{\mathrm{ofs}} = \lambda_0 - \lambda_{\mathrm{ZDW}} = 10$ nm.

Optics EXPRESS

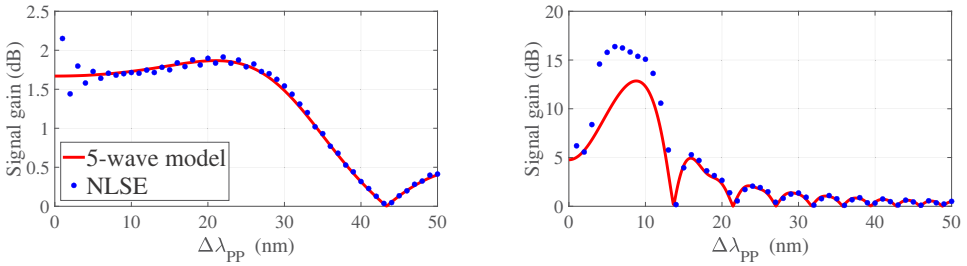

(a) L = 100 m. (b) L = 720 m.

Fig. 3. Plot of maximum PSA signal gain using the five-wave model (red solid line) and NLSE (blue filled circles) as a function of the pump-pump wavelength separation $\Delta\lambda_{PP}$, for two different fiber lengths, (a) 100 m and (b) 720 m. Other parameters: $\gamma = 11.3\ \mathrm{W}^{-1}.\mathrm{km}^{-1}$, $\lambda_{ZDW} = 1547.5$ nm, $D' = 0.017\ \mathrm{ps.nm}^{-2}.\mathrm{km}^{-1}$, pump powers $P = 20$ dBm, signal input power −20 dBm, signal wavelength $\lambda_0 = 1557.5$ nm, $\delta\lambda_{ofs} = 10$ nm.

Figure 3 compares two different models: the analytical five-wave model (red full line) plotted using Eq. (3) and the NLSE based model (blue dotted line). One can see that for a small value of the fiber length $L = 100$ m, there is a good agreement between the five-wave model and the NLSE. This proves that the hypotheses done to obtain Eq. (2) are not too crude, at least in this domain of parameters. However, for a longer fiber length ($L = 720$ m), the NLSE predicts a different signal gain compared to the five-wave model for small pump-pump wavelength separations ($\Delta\lambda_{PP}$<12 nm). This feature is related to the emergence of extra waves beyond the five waves, leading the five-wave model to fail in this case. Conversely, for $\Delta\lambda_{PP}$>12 nm, both models end up giving the same signal gain because the extra waves become negligible in this regime, since the FWM processes that create them become strongly phase mismatched. The periodic zeroes in the gain spectrum are characteristic of any parametric amplifier arising due to perfect phase mismatching at certain values of $\Delta\lambda_{PP}$ [34].

Corresponding to the gain, the NF values are shown in Figs. 4(a,b). For the short fiber length ($L = 100$ m), Fig. 4(a) reproduces the evolution of the NF versus $\Delta\lambda_{PP}$ according to both the quantum five-wave model and the semi-classical model based on the NLSE. However, for the longer fiber length ($L = 720$ m), we only provide in Fig. 4(b) the NF obtained from the NLSE approach as the five-wave model is not valid in this regime. The signal NF in the case of the five-wave model (full red line) is calculated from Eq. (7) by using the input signal phase values θ_0 that maximize the signal gain, whereas it is obtained in the case of the NLSE (blue dotted line) from Eq. (9) by considering the maximized value of the three partial derivatives after varying the phase of the input fluctuations in the three waves. For example, we show in Fig. 5 how the output signal (Fig. 5(a)), HOI1 (Fig. 5(b)) and HOI2 (Fig. 5(c)) powers change with the square root of the power of the input wave that mimics the noise of the input wave. In fact, the slope of the curve depends also on the phase of the input injected "noise", as can be seen from the red (phase = 0.2 rad), blue (phase = 1 rad) and green (phase = 2.3 rad) curves in Fig. 5. For the NF calculation using Eq. (9), we always consider the phase of the injected "noise" that maximizes the slope of these curves.

Similarly to the preceding discussion about the gain, Fig. 4(a) shows that the five-wave quantum NF agrees satisfactorily with the NF based on NLSE (for a length of 100 m), except for very small values of $\Delta\lambda_{PP}$ where the NLSE model shows an increase of the NF with respect to the five-wave model due to the existence of higher order waves beyond the five waves. In fact, for a 100 m fiber, the NF values calculated from these two models are also confirmed with a five-wave numerical approach similar to Ref. [21] (see Supplement 1).

Optics EXPRESS

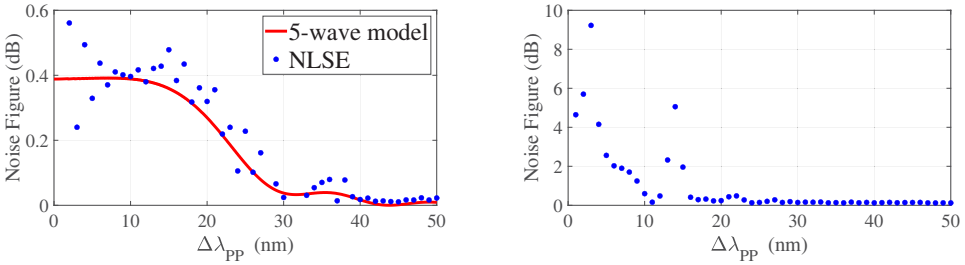

(a) L = 100 m. (b) L = 720 m.

Fig. 4. Plot of signal NF using the five-wave model (red solid line) and NLSE (blue filled circles) as a function of the pump-pump wavelength separation according to both the quantum five-wave model and the semi-classical model based on the NLSE. Fiber lengths, (a) 100 m and (b) 720 m. Other parameters are same as Fig. 3.

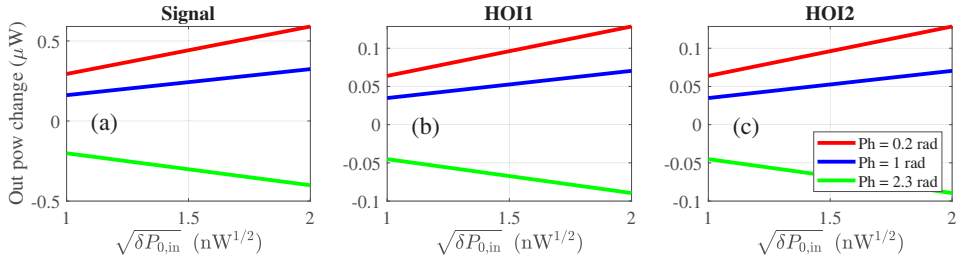

Fig. 5. Plot of output power change of (a) the signal, (b) HOI1, and (c) HOI2 as a function of the square root of the input injected signal noise power $\delta P_{0,\text{in}}$, for three different noise phases 0.2 rad (red), 1 rad (blue) and 2.3 rad (green). L = 100 m, $\Delta\lambda_{PP}$ = 10 nm.

Figure 4(b) also shows that the existence of high-order waves leads to an increase of the NF with respect to what is expected from the well-known value of the three-wave model (0 dB). This increase is due to input vacuum fluctuations that are injected in the high-order waves at the fiber input. Indeed, during the amplification process, these vacuum noises are transferred to the signal through nonlinear FWM processes, thus potentially degrading the NF. However, a good trade off between the gain increase and the NF degradation is reached here. Indeed, when the signal gain is maximum around $\Delta\lambda_{PP}$ = 6 nm (blue dotted curve in Fig. 3(b)) a small degradation of the NF (around 2 dB in Fig. 4(b)) is expected using the semi-classical approach based NLSE model. This can be explained by the fact that in this region the dominant FWM processes for the growth of the signal are the ones that exchange power from one mode to the other modes at different frequencies. Since these processes are known to be noiseless, no vacuum noises are transferred from the high-order idlers to the signal mode through these processes.

Notice also that the local peak in Fig. 4(b) around $\Delta\lambda_{PP}$ = 12 nm arises due to the zero of the maximum signal gain around this value.

To summarize, this result shows that one can take advantage of the emergence of the high-order waves to enhance the signal gain, while maintaining the NF of the amplifier around 2 dB, which is much below the 3 dB limit encountered in the case of a three-wave phase insensitive amplifier. This was already observed in Ref. [21], but in the framework of the semi-classical seven-wave approach. The present work confirms this result using a NLSE-based model and that is validated using a more rigorous fully quantum approach.

Optics EXPRESS

3.4. Discussion

As already discussed in Sections 3.1 and 3.2, a difference between the quantum-mechanical and semi-classical pictures is that the quantum noise in the former one appears as an inherent property of the field, while for the latter one it has to be introduced as an extra noise term. Hence, in terms of noise figure calculations, the quantum description of noise is more accurate. However, Section 3.1 has shown that the quantum-mechanical approach is applicable only when the coupled equations describing the evolution of the interacting waves can be solved analytically, and thus an input-output relation can be derived. This is achieved only in the unsaturated gain regime, in which the pumps remain undepleted along propagation. On the contrary, for the saturated gain regime, in which the other waves become strong enough to deplete the pump powers significantly, analytical solutions are in general no longer available. Then the noise properties of parametric processes can no longer be treated quantum mechanically. As an alternative, a semi-classical approach is commonly used, which is a simple yet rigorous translation of some quantum statements. Indeed, the main feature of this approach compared to its quantum counterpart is that numerical simulations can be carried out in the strong pump depletion regime. Hence the noise figure can be calculated in the saturation regime. Another feature is that the noise properties of the pumps can be also investigated, contrary to the quantum-mechanical approach that always treats the pumps classically.

Even though the two approaches are conceptually rather different, it has been proved that in the large photon-number approximation, both of them are of comparable accuracy. This result has been proved in the case of the fundamental three-wave model [32,35,36]. In the previous Subsection 3.3, we have shown from Fig. 4 that the two approaches are in good agreement in the framework of the multi-wave model as well, when the photon numbers are large, but only to the extent when the system nonlinearity is weak (see Fig. 4(a)). However in the case of larger nonlinearity, i.e. Figure 4(b), when the pump-pump separation is small, only the semi-classical approach using the NLSE can be used since the analytical approach is oblivious of the existence of the high-order waves [18]. This conclusion is important when it comes to studying noise properties of more complex systems, for which quantum calculations cannot be applied by lack of analytical solutions, and where only semi-classical calculations can be carried out instead.

4. Conversion efficiency (CE) and noise figure (NF) of PSFC

In order to effectively utilize a dual-pump PSFC as described in Subsection 2.2 (see Fig. 2), it is important to study its properties with respect to the relevant system parameters. Here we study two properties *viz.* the conversion efficiency (CE) and the noise figure (NF) associated with the frequency conversion, as described below.

4.1. Conversion efficiency

As previously discussed in Subsection 2.2, the CE is the ratio of the output power of the signal (or HOI2) to the input power of the HOI1. Thus we first compare the obtained CE of a PSFC from the analytical five-wave model and NLSE approaches for two different fiber lengths in Fig. 6. All the numerical and system parameters are the same as mentioned in Subsection 3.3 except that here, instead of the input signal power, the input HOI1 power is −20 dBm. No input power is launched in the signal mode.

Firstly, we see from Fig. 6 that the output powers of the signal and HOI2 are sensitive to the input phase of HOI1, showing the phase sensitivity of the system CE [37]. Secondly, from Fig. 6 we see that although for a smaller length (100 m) of the fiber, the CE obtained from the five-wave model and the NLSE agree with each other (see Fig. 6(a)), once the length is larger (720 m), the two models deviate (see Fig. 6(b)). This is because for longer fiber lengths, the influence of the high-order waves starts impacting the wave evolution process [4,18]. Since the effects

Optics EXPRESS

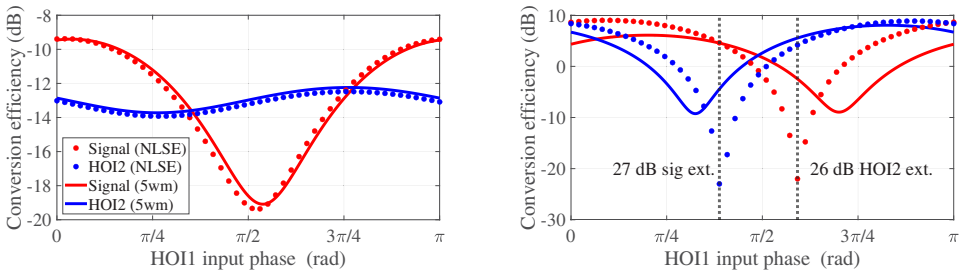

(a) L = 100 m. (b) L = 720 m.

Fig. 6. Plot of conversion efficiency of signal (red) and HOI2 (blue) from the five-wave model (solid line) and NLSE (filled circles) as a function of the input HOI1 phase, for two different fiber lengths, (a) 100 m and (b) 720 m. The HOI1 input phases corresponding to highest signal and HOI2 extinction ratios are marked with dashed lines. $\Delta\lambda_{PP}$ = 7 nm, $\delta\lambda_{ofs}$ = 10 nm.

of these high-order waves are only considered in the NLSE model, we stick to this model for the subsequent analysis of the CE in the PSFC process for longer fiber lengths. The utility of the analytical five-wave model lies in the validation of the semi-classical NLSE based approach for shorter fiber lengths where the analytical model is valid. From Fig. 6(a) we also notice that the phase-sensitivity of the HOI2 is much lower than that of the signal. On the contrary, in Fig. 6(b), when the length is larger, both the signal and the HOI2 show almost equal levels of phase-sensitivity. This is due to the fact that for a shorter fiber, the HOI2 is farther in frequency from the HOI1 compared to the signal, and hence it is weakly coupled to HOI1. However, for a longer fiber, where the signal is efficiently generated, the coupling of HOI2 to the HOI1 can easily be mediated through the signal. Thus it can be sensitive to the input phase of HOI1.

As one might expect, here our primary motive in terms of PSFC functionality is to optimize the system parameters such that both the signal (or HOI2) output power and the signal-HOI2 (or HOI2-signal) extinction ratio are maximized. To this aim, in Fig. 7 we show the false color plots of the output signal power (top row), HOI2 power (middle row) and signal-to-HOI2 extinction ratio (bottom row) as a function of the input HOI1 phase and the fiber length, computed by numerically solving the NLSE, for different values of $\delta\lambda_{ofs}$, namely (a,d,g) $\delta\lambda_{ofs} = -10$ nm, (b,e,h) $\delta\lambda_{ofs} = 1$ nm and (c,f,i) $\delta\lambda_{ofs} = 10$ nm. The pump-pump wavelength separation $\Delta\lambda_{PP}$ is 7 nm. Note that by varying the fiber length, we are effectively changing the nonlinear phase γPL added by the HNLF to the different propagating waves [38].

From Fig. 7 we see that the most interesting case arises around $\delta\lambda_{ofs} = 1$ nm and a fiber length of 720 m (see Figs. 7(b),(e),(h)), where an efficient frequency conversion is predicted. In this case, when the input phase of HOI1 is close to $\frac{3\pi}{8}$, the HOI1 wave is converted preferably to the signal wave, with a signal-HOI2 extinction ratio of the order of 20 dB. On the contrary, when the input phase is close to $\frac{5\pi}{8}$, HOI1 is converted mainly to HOI2, with a similar HOI2-signal extinction ratio. We also note here that the level of phase control required to maintain an extinction ratio above 20 dB is typically around 0.06 rad. Another interesting feature of Fig. 7 is the strong dependence of the signal-HOI2 extinction ratio on the fiber length and $\delta\lambda_{ofs}$. In Fig. 7(h) we can see two localized blobs (see the regions where the grey dashed lines intersect) that denote efficient PSFC of the signal or the HOI2. We can also notice that across the different subfigures in Fig. 7, the position and conspicuity of these blobs vary. These blobs, that probably arise out of singular solutions of the NLSE, line up with respect to the fiber length, only for the case of $\delta\lambda_{ofs} = 1$ nm at 720 m fiber length. Typically we want these blobs to be apart by $\frac{\pi}{2}$ radians, in terms of input HOI1 phase, such that switching from production of signal to HOI2 at the output does not require very precise control over the HOI1 input phase. Although for Fig. 7(h) the phase

Optics EXPRESS

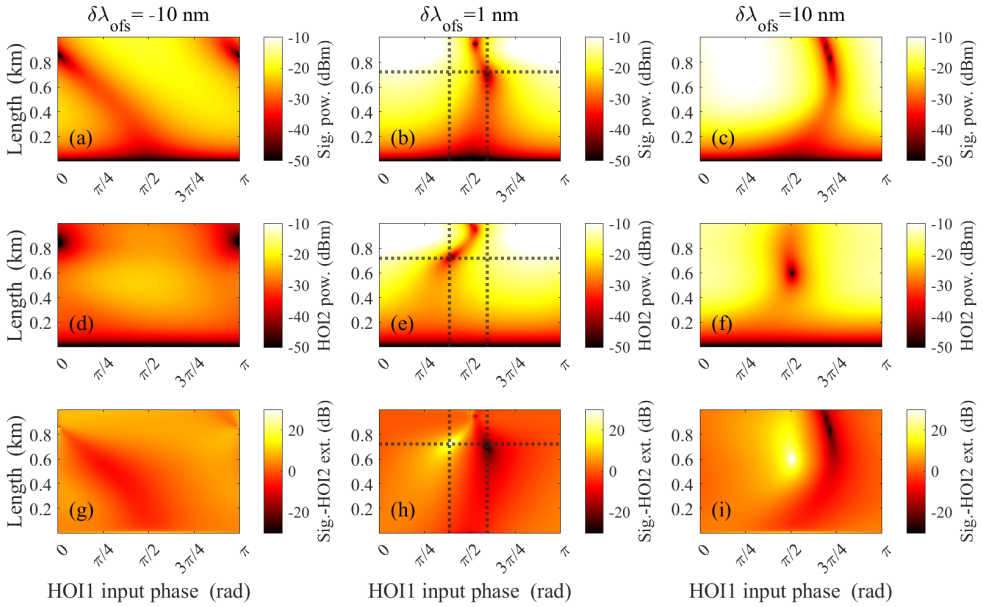

Fig. 7. False color plots of output signal power (top row), HOI2 power (middle row) and signal-to-HOI2 extinction ratio (bottom row) as a function of the input HOI1 phase and the fiber length, for different values of $\delta\lambda_{\text{ofs}}$. (a,d,g) $\delta\lambda_{\text{ofs}} = -10$ nm, (b,e,h) $\delta\lambda_{\text{ofs}} = 1$ nm and (c,f,i) $\delta\lambda_{\text{ofs}} = 10$ nm. NLSE simulation was used to generate the data. Positions of high extinction ratio extrema in (b,e,h) are indicated with grey dashed lines. Horizontal dashed line corresponds to a fiber length of 0.72 km. $\Delta\lambda_{\text{PP}} = 7$ nm.

separation is not exactly $\frac{\pi}{2}$, but $\frac{\pi}{4}$, it is nevertheless an optimal case of an efficient PSFC for the considered system.

Having investigated the system CE performance with respect to $\delta\lambda_{\text{ofs}}$, now we fix $\delta\lambda_{\text{ofs}}$ at a value of 1 nm, and show the corresponding plots in Fig. 8 for different values of $\Delta\lambda_{\text{PP}}$, namely Figs. 8(a),(d),(g) 5 nm, (b),(e),(h) 7 nm, and (c),(f),(i) 9 nm. For these three different values of $\Delta\lambda_{\text{PP}}$, we obtain reasonably good frequency conversion as can be seen from Figs. 8(g),(h),(i). However the best case turns out to be $\Delta\lambda_{\text{PP}} = 7$ nm, where the blobs are better lined up with respect to fiber length (at 720 m) and are better separated with respect to HOI1 input phase. Therefore from our numerical analysis, we find that an optimal design of a dual-pump PSFC would require $L = 720$ m, $\Delta\lambda_{\text{PP}} = 7$ nm, and $\delta\lambda_{\text{ofs}} = 1$ nm.

4.2. *Noise figure associated with frequency conversion*

Apart from the CE, the quality of an active frequency converter also depends on the associated noise. Thus following our previous developments, here we investigate the NF coming with the PSFC using the quantum and semi-classical models already introduced in Section 3.

4.2.1. Quantum-mechanical NF based on the five-wave model

In our discussed PSFC model, when the launched HOI1 ($j = -2$) gets converted to either the signal ($j = 0$) or the HOI2 ($j = 2$), the noise in the input HOI1 mode is also transferred to the converted modes. The extra noise due to PSFC in the j-th output mode is characterized by the noise figure (NF_j) given by:

$$\text{NF}_j = \frac{\langle N_{-2}\rangle_{\text{in}}^2}{\langle \Delta N_{-2}^2\rangle_{\text{in}}} \cdot \frac{\langle \Delta N_j^2\rangle_{\text{out}}}{\langle N_j\rangle_{\text{out}}^2} \,. \tag{12}$$

Optics EXPRESS

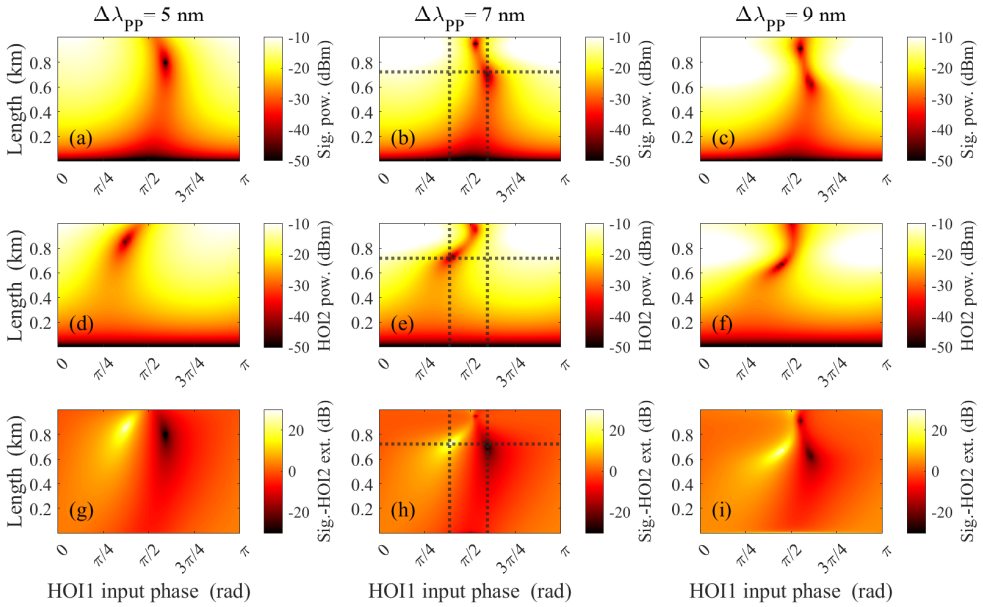

Fig. 8. Same as Fig. 7, but for different $\Delta\lambda_{PP}$'s. (a,d,g) $\Delta\lambda_{PP}$ = 5 nm, (b,e,h) $\Delta\lambda_{PP}$ = 7 nm and (c,f,i) $\Delta\lambda_{PP}$ = 9 nm. $\delta\lambda_{ofs}$ = 1 nm.

Note that NF_j is nothing but the ratio of the input and output signal-to-noise ratios before and after frequency conversion to the j-th mode.

Similarly to Subsection 3.1 and Eq. (7), here also we make use of the *Mathematica* code provided in the supplementary information to calculate the NF_j expressions for the signal and the HOIs. In the case where only HOI1 is present at the input, the initial quantum state of the system is given by $|\psi\rangle = |0_0, \alpha_{-2}, 0_2\rangle$. By assuming that $|\alpha_{-2}|^2 \gg 1$, NF_j (for $j = -2, 0, 2$) is given by :

$$
\begin{aligned}
\mathrm{NF}_j = \frac{1}{\left(|\mu_{k3}|^2 + |\mu_{k4}|^2 + 2|\mu_{k4}||\mu_{k3}|\cos(2\theta_{-2} + \theta_{k3} - \theta_{k4})\right)^2} \times \Big\{ & |\mu_{k3}|^4 + |\mu_{k4}|^4 + 6|\mu_{k4}|^2|\mu_{k3}|^2 \\
& + |\mu_{k5}|^2|\mu_{k3}|^2 + |\mu_{k6}|^2|\mu_{k3}|^2 + |\mu_{k1}|^2|\mu_{k4}|^2 + |\mu_{k2}|^2|\mu_{k4}|^2 + |\mu_{k4}|^2|\mu_{k5}|^2 + |\mu_{k4}|^2|\mu_{k6}|^2 \\
& + |\mu_{k1}|^2|\mu_{k3}|^2 + |\mu_{k2}|^2|\mu_{k3}|^2 + 4|\mu_{k4}||\mu_{k3}|^3\cos(2\theta_{-2} + \theta_{k3} - \theta_{k4}) \\
& + 2|\mu_{k1}||\mu_{k2}||\mu_{k3}|^2\cos(2\theta_{-2} - \theta_{k1} - \theta_{k2} + 2\theta_{k3}) + 2|\mu_{k5}||\mu_{k6}||\mu_{k3}|^2\cos(2\theta_{-2} + 2\theta_{k3} - \theta_{k5} - \theta_{k6}) \\
& + 4|\mu_{k1}||\mu_{k2}||\mu_{k4}||\mu_{k3}|\cos(\theta_{k1} + \theta_{k2} - \theta_{k3} - \theta_{k4}) + 4|\mu_{k4}|^3|\mu_{k3}|\cos(2\theta_{-2} + \theta_{k3} - \theta_{k4}) \\
& + 2|\mu_{k4}||\mu_{k5}|^2|\mu_{k3}|\cos(2\theta_{-2} + \theta_{k3} - \theta_{k4}) + 2|\mu_{k4}||\mu_{k6}|^2|\mu_{k3}|\cos(2\theta_{-2} + \theta_{k3} - \theta_{k4}) \\
& + 2|\mu_{k1}|^2|\mu_{k4}||\mu_{k3}|\cos(2\theta_{-2} + \theta_{k3} - \theta_{k4}) + 2|\mu_{k2}|^2|\mu_{k4}||\mu_{k3}|\cos(2\theta_{-2} + \theta_{k3} - \theta_{k4}) \\
& + 4|\mu_{k4}||\mu_{k5}||\mu_{k6}||\mu_{k3}|\cos(\theta_{k3} + \theta_{k4} - \theta_{k5} - \theta_{k6}) + 2|\mu_{k1}||\mu_{k2}||\mu_{k4}|^2\cos(2\theta_{-2} + \theta_{k1} + \theta_{k2} - 2\theta_{k4}) \\
& + 2|\mu_{k4}|^2|\mu_{k5}||\mu_{k6}|\cos(2\theta_{-2} - 2\theta_{k4} + \theta_{k5} + \theta_{k6})\Big\},
\end{aligned}
\tag{13}
$$

where $|\mu_{kl}|$ is the modulus of the complex coefficient μ_{kl} and θ_{kl} its argument, with $l = 1..6$, and $k = 1, 3, 5$ when $j = 0, -2, 2$, respectively. θ_{-2} is the input phase of the HOI1 launched at the fiber input. The exact expressions of the μ_{kl}'s (as given in Eq. (2)) can be obtained from [4].

Equation (13) can be interpreted in a similar way as Eq. (7). The difference lies in the presence of the HOI1 mode at the input instead of the signal mode, which gives rise to the dependence of the NF on the input HOI1 phase θ_{-2}. All the terms in this equation can similarly be explained as

Optics EXPRESS

in Eq. (7). For example, if we take $j = -2$ with $k = 3$ in Eq. (13), all the terms depend on the coefficients $|\mu_{3l}|$ of the third row of the transfer matrix (Eq. (2)) linking the output HOI1 to the input signal, HOI1 and HOI2. Then, depending on the index $l = 1, ..6$, one can distinguish the different nonlinear couplings occurring between the interacting modes.

Here also, the dependence of some terms on the input HOI1 phase confirms the phase sensitive frequency conversion capability of this scheme.

4.2.2. Semi-classical NF based on NLSE

Similarly to the analysis described in Subsection 3.2, we write the semi-classical NF expression of the signal ($j = 0$) and HOI2 ($j = 2$) following Ref. [21]. In a way analogous to Eq. (9), NF_j is given by (see Supplement 1) :

$$\mathrm{NF}_j = \frac{1}{4{G_j}^2 P_{-2,\mathrm{in}}} \left[\left(\frac{\partial P_{j,\mathrm{out}}}{\partial \sqrt{P_{-2,\mathrm{in}}}} \right)^2 + \left(\frac{\partial P_{j,\mathrm{out}}}{\partial \sqrt{P_{0,\mathrm{in}}}} \right)^2 + \left(\frac{\partial P_{j,\mathrm{out}}}{\partial \sqrt{P_{2,\mathrm{in}}}} \right)^2 \right], \tag{14}$$

where $P_{j,\mathrm{in}}$ and $P_{j,\mathrm{out}}$ are the input and output powers of the j-th wave, respectively. G_j is the relative gain of the j-th wave with respect to input HOI1 power :

$$G_j(\theta_{-2}) = \frac{P_{j,\mathrm{out}}}{P_{-2,\mathrm{in}}}. \tag{15}$$

Note that the three terms in Eq. (14) correspond to the differential transfer to the considered output mode of the fluctuations at the input of the three (HOI1, signal, and HOI2) considered modes.

From Eq. (14), we evaluate the signal and HOI2 NF as a function of the input HOI1 phase. The derivatives are computed using the NLSE simulation, by injecting different amounts of power mimicking the noise at the input of the signal, HOI1 and HOI2, and extracting the corresponding slopes. Since the system is highly phase sensitive, it is important to consider the phase of the input injected "noise" that maximizes the photon transfer to the j-th mode. In each case, we thus scan the phase of the injected mode and keep the maximum slope to evaluate the three partial derivatives and thereafter calculate the values of NF_j.

4.2.3. Comparison between the approaches

In order to calculate the NF of the PSFC, we again consider two different fiber lengths, $L = 100$ m and $L = 720$ m. For $L = 100$ m, we plot the evolution of the NF for the signal (in red) and HOI2 (in blue) versus input phase of HOI1, as shown in Fig. 9(a). For this short fiber length, Fig. 9(a) also compares the two approaches (semi-classical NLSE and quantum five-wave model) used to calculate the NF. As one might expect, since the system nonlinearity is weak in this case, the NLSE based (filled circles) and five-wave model based (solid line) approaches agree very well with each other. This agreement between the models at low system nonlinearity allows us to extend the NLSE based approach to longer fiber lengths, for which the larger nonlinearity makes the five-wave model irrelevant. An example of such a calculation is shown in Fig. 9(b) for $L = 720$ m. One notices that for such a longer fiber length, the minimum NF of the signal is predicted to be around 5 dB. For the shorter length however, when the gain is low, we find the minimum NF values to be much larger, *i.e.* around 10 dB and 12 dB for the signal and HOI2, respectively.

4.2.4. Discussion

From the graphs of Fig. 9, it is clear that each time the HOI1 is efficiently converted either to the signal or to HOI2 (compare Fig. 6 with Fig. 9), then the associated NF is small. Consequently, this scheme also provides the possibility to convert an incoming HOI1 wave to the wave with a lower NF (either signal or HOI2), just by modifying the HOI1 input phase.

Optics EXPRESS

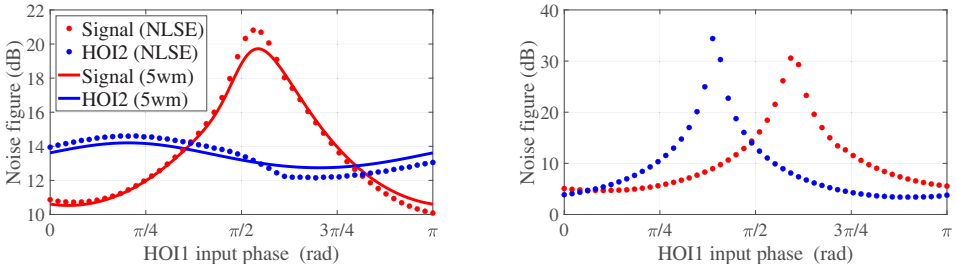

(a) L = 100 m. (b) L = 720 m.

Fig. 9. Noise figure of signal (red) and HOI2 (blue) using the five-wave model (solid line) and NLSE (filled circles), as a function of input phase of HOI1 for fiber lengths (a) 100 m and (b) 720 m. Same parameters as in Fig. 6. The parameters used are the optimized parameters that lead to an efficient PSFC : L = 720 m, $\Delta\lambda_{\mathrm{PP}}$ = 7 nm and $\delta\lambda_{\mathrm{ofs}}$ = 10 nm.

5. Conclusion

In this work, we have primarily investigated the gain and noise figure characteristics of a phase sensitive frequency converter based on two pumps. We have shown theoretically that this system can be optimized in such a way that by launching the input wave into the HOI1 channel at the fiber input, and by adjusting the initial phase of the HOI1, the signal can be preferentially converted to the signal and HOI2 channels. This shows that the system is capable of operating as a phase sensitive frequency converter. The evaluation of the noise figure of such a system was performed using a semi-classical model, where the system is numerically solved using the NLSE, and the mode noises are injected as classical fluctuations of the complex field amplitude with a zero mean and a variance of half a photon. This semi-classical model was also validated using a fully quantum model for a short fiber length, *i.e.*, a weak nonlinearity.

In the PSFC case, we also numerically investigated the conversion efficiencies of the system into signal and HOI2 from HOI1, with respect to the the pump-pump wavelength separation $\Delta\lambda_{\mathrm{PP}}$, signal detuning from the fiber zero-dispersion wavelength $\delta\lambda_{\mathrm{ofs}}$ and the fiber length L, by solving the NLSE numerically. We found the optimized parameters to be $\Delta\lambda_{\mathrm{PP}}$ = 7 nm, $\delta\lambda_{\mathrm{ofs}}$ = 1 nm and L = 720 m for an extinction ratio of 20 dB. As a perspective of this work, we can extend similar analysis for PSA and PSFC in dispersion tailored fibers as well [37].

Finally, we believe that this paper opens new avenues for further research in calculating and optimizing the noise figure of more complex PSA systems, where semi-classical calculations can be used in the absence of analytical solutions. It should stimulate further experimental efforts towards the design of optical frequency converters with only two pump waves, where an adjustment of the pump phases is not necessary.

Acknowledgments. The authors are happy to thank I. Fsaifes and W. Xie for their interest in the early stages of this work.

Disclosures. The authors declare no conflicts of interest.

Data availability. Data underlying the results presented in this paper are not publicly available at this time but may be obtained from the authors upon reasonable request.

Supplemental document. See Supplement 1 for supporting content.

References

1. J. Ma, J. Yu, C. Yu, Z. Jia, X. Sang, Z. Zhou, T. Wang, and G. K. Chang, "Wavelength conversion based on four-wave mixing in high-nonlinear dispersion shifted fiber using a dual-pump configuration," J. Lightwave Technol. **24**(7), 2851–2858 (2006).

Optics EXPRESS

2. F. Da Ros, K. Dalgaard, L. Lei, J. Xu, and C. Peucheret, "QPSK-to-2×BPSK wavelength and modulation format conversion through phase-sensitive four-wave mixing in a highly nonlinear optical fiber," Opt. Express **21**(23), 28743–28750 (2013).
3. M. Baillot, M. Gay, C. Peucheret, J. Michel, and T. Chartier, "Phase quadrature discrimination based on three-pump four-wave mixing in nonlinear optical fibers," Opt. Express **24**(23), 26930–26941 (2016).
4. D. Chatterjee, Y. Bouasria, F. Goldfarb, and F. Bretenaker, "Analytical seven-wave model for wave propagation in a degenerate dual-pump fiber phase sensitive amplifier," J. Opt. Soc. Am. B **38**(4), 1112–1124 (2021).
5. R. Slavík, F. Parmigiani, J. Kakande, C. Lundström, M. Sjödin, P. A. Andrekson, R. Weerasuriya, S. Sygletos, A. D. Ellis, L. Grüner-Nielsen, D. Jacobsen, S. Herstrøm, R. Phelan, J. O'Gorman, A. Bogris, D. Syvridis, S. Dasgupta, P. Petropoulos, and D. J. Richardson, "All-optical phase and amplitude regenerator for next-generation telecommunications systems," Nat. Photonics **4**(10), 690–695 (2010).
6. Z. Tong, C. Lundström, P. Andrekson, C. McKinstrie, M. Karlsson, D. Blessing, E. Tipsuwannakul, B. Puttnam, H. Toda, and L. Grüner-Nielsen, "Towards ultrasensitive optical links enabled by low-noise phase-sensitive amplifiers," Nat. Photonics **5**(7), 430–436 (2011).
7. R. Webb, J. Dailey, R. Manning, and A. Ellis, "Phase discrimination and simultaneous frequency conversion of the orthogonal components of an optical signal by four-wave mixing in an soa," Opt. Express **19**(21), 20015–20022 (2011).
8. R. Webb, M. Power, and R. Manning, "Phase-sensitive frequency conversion of quadrature modulated signals," Opt. Express **21**(10), 12713–12727 (2013).
9. J. Zhou, N. Park, J. W. Dawson, K. J. Vahala, M. A. Newkirk, and B. I. Miller, "Efficiency of broadband four-wave mixing wavelength conversion using semiconductor traveling-wave amplifiers," IEEE Photonics Technol. Lett. **6**(1), 50–52 (1994).
10. Y. Wang, C. Yu, T. Luo, L. Yan, Z. Pan, and A. E. Willner, "Tunable all-optical wavelength conversion and wavelength multicasting using orthogonally polarized fiber fwm," J. Lightwave Technol. **23**(10), 3331–3338 (2005).
11. A. Vedadi, M. E. Marhic, E. Lantz, H. Maillotte, and T. Sylvestre, "Investigation of gain ripple in two-pump fiber optical parametric amplifiers," Opt. Lett. **33**(19), 2203–2205 (2008).
12. M. Marhic, A. Rieznik, and H. Fragnito, "Investigation of the gain spectrum near the pumps of two-pump fiber-optic parametric amplifiers," J. Opt. Soc. Am. B **25**(1), 22–30 (2008).
13. M. Gao, T. Inoue, T. Kurosu, and S. Namiki, "Evolution of the gain extinction ratio in dual-pump phase sensitive amplification," Opt. Lett. **37**(9), 1439–1441 (2012).
14. M. Baillot, T. Chartier, and M. Joindot, "Multiple four-wave mixing in optical fibres," in *2014 The European Conference on Optical Communication (ECOC)*, (IEEE, 2014), pp. 1–3.
15. J. Qian, M. Gao, L. Xiang, and G. Shen, "Investigation of high gain dual-pump phase sensitive amplifiers," Optik **135**, 210–218 (2017).
16. Y. Bouasria, D. Chatterjee, F. Goldfarb, Y. Hassouni, and F. Bretenaker, "Generalised expression of the noise figure of phase sensitive amplifiers for an arbitrary number of modes," Journal of Optics (2020).
17. C. J. McKinstrie, S. Radic, and M. Raymer, "Quantum noise properties of parametric amplifiers driven by two pump waves," Opt. Express **12**(21), 5037–5066 (2004).
18. W. Xie, I. Fsaifes, T. Labidi, and F. Bretenaker, "Investigation of degenerate dual-pump phase sensitive amplifier using multi-wave model," Opt. Express **23**(25), 31896–31907 (2015).
19. W. Xie, I. Fsaifes, and F. Bretenaker, "Optimization of a degenerate dual-pump phase-sensitive optical parametric amplifier for all-optical regenerative functionality," Opt. Express **25**(11), 12552–12565 (2017).
20. K. Inoue, "Influence of multiple four-wave-mixing processes on quantum noise of dual-pump phase-sensitive amplification in a fiber," J. Opt. Soc. Am. B **36**(6), 1436–1446 (2019).
21. Y. Bouasria, D. Chatterjee, W. Xie, I. Fsaifes, F. Goldfarb, Y. Hassouni, and F. Bretenaker, "Investigation of the noise figure in a degenerate dual-pump phase-sensitive amplifier using a multi-wave model," J. Opt. Soc. Am. B **37**(9), 2745–2754 (2020).
22. D. Chatterjee, Y. Bouasria, F. Goldfarb, and F. Bretenaker, "Analytical modeling of phase sensitive frequency conversion with a nonlinear fiber in a dual pump architecture," in *Nonlinear Optics*, (Optical Society of America, 2021), pp. NF2A–8.
23. M. E. Marhic, *Fiber optical parametric amplifiers, oscillators and related devices* (Cambridge university press, 2008).
24. Y. Chen and A. W. Snyder, "Four-photon parametric mixing in optical fibers: effect of pump depletion," Opt. Lett. **14**(1), 87–89 (1989).
25. W. Louisell, A. Yariv, and A. Siegman, "Quantum fluctuations and noise in parametric processes. I," Phys. Rev. **124**(6), 1646–1654 (1961).
26. H. A. Haus and J. Mullen, "Quantum noise in linear amplifiers," Phys. Rev. **128**(5), 2407–2413 (1962).
27. J. Gordon, W. H. Louisell, and L. R. Walker, "Quantum fluctuations and noise in parametric processes. II," Phys. Rev. **129**(1), 481–485 (1963).
28. C. M. Caves, "Quantum limits on noise in linear amplifiers," Phys. Rev. D **26**(8), 1817–1839 (1982).
29. J. A. Levenson, I. Abram, T. Rivera, and P. Grangier, "Reduction of quantum noise in optical parametric amplification," J. Opt. Soc. Am. B **10**(11), 2233–2238 (1993).

Optics EXPRESS

30. Z. Tong, C. McKinstrie, C. Lundström, M. Karlsson, and P. A. Andrekson, "Noise performance of optical fiber transmission links that use non-degenerate cascaded phase-sensitive amplifiers," Opt. Express **18**(15), 15426–15439 (2010).
31. Z. Tong, C. Lundström, P. A. Andrekson, M. Karlsson, and A. Bogris, "Ultralow noise, broadband phase-sensitive optical amplifiers, and their applications," IEEE J. Sel. Top. Quantum Electron. **18**(2), 1016–1032 (2012).
32. S. Donati and G. Giuliani, "Noise in an optical amplifier: Formulation of a new semiclassical model," IEEE J. Quantum Electron. **33**(9), 1481–1488 (1997).
33. H. Pakarzadeh, R. Golabi, and C. Peucheret, "Two-pump fiber optical parametric amplifiers: Beyond the 6-wave model," Opt. Fiber Technol. **45**, 223–230 (2018).
34. G. P. Agrawal, "Nonlinear fiber optics," in *Nonlinear Science at the Dawn of the 21st Century*, (Springer, 2000), pp. 195–211.
35. M. Shtaif, B. Tromborg, and G. Eisenstein, "Noise spectra of semiconductor optical amplifiers: Relation between semiclassical and quantum descriptions," IEEE J. Quantum Electron. **34**(5), 869–878 (1998).
36. S. M. M. Friis, K. Rottwitt, and C. McKinstrie, "Raman and loss induced quantum noise in depleted fiber optical parametric amplifiers," Opt. Express **21**(24), 29320–29331 (2013).
37. D. Chatterjee, A. Konyukhov, A. Sysoliatin, and D. Venkitesh, "Phase-sensitive amplification in a dispersion oscillating fiber with two pumps," in *Asia Communications and Photonics Conference*, (Optical Society of America, 2021), pp. W2A–3.
38. L. Wang, M. Gao, M. Liu, H. Zhu, B. Chen, and L. Xiang, "Energy-efficient all optical wavelength converter for optical phase conjugation," Opt. Fiber Technol. **58**, 102278 (2020).